ARL-TR-7399 ● AUG 2015

US Army Research Laboratory

Effect of Atomic Layer Depositions (ALD)-Deposited Titanium Oxide (TiO_2) Thickness on the Performance of $Zr_{40}Cu_{35}Al_{15}Ni_{10}$ (ZCAN)/ TiO_2/Indium (In)-Based Resistive Random Access Memory (RRAM) Structures

by Matthew L Chin, Matin Amani, Terrence P O'Regan, A Glen Birdwell, and Madan Dubey

NOTICES

Disclaimers

ARL-TR-7399 ● AUG 2015

US Army Research Laboratory

Effect of Atomic Layer Depositions (ALD)-Deposited Titanium Oxide (TiO_2) Thickness on the Performance of $Zr_{40}Cu_{35}Al_{15}Ni_{10}$ (ZCAN)/ TiO_2/Indium (In)-Based Resistive Random Access Memory (RRAM) Structures

by Matthew L Chin, Matin Amani, Terrence P O'Regan, A Glen Birdwell, and Madan Dubey
Sensors and Electron Devices Directorate, ARL

REPORT DOCUMENTATION PAGE					*Form Approved* *OMB No. 0704-0188*

1. REPORT DATE *(DD-MM-YYYY)* Aug 2015	**2. REPORT TYPE** Final	**3. DATES COVERED (From - To)** 09/2014
4. TITLE AND SUBTITLE Effect of Atomic Layer Depositions (ALD)-Deposited Titanium Oxide (TiO_2) Thickness on the Performance of $Zr_{40}Cu_{35}Al_{15}Ni_{10}$ (ZCAN)/ TiO_2/Indium (In)-Based Resistive Random Access Memory (RRAM) Structures		**5a. CONTRACT NUMBER**
		5b. GRANT NUMBER
		5c. PROGRAM ELEMENT NUMBER
6. AUTHOR(S) Matthew L Chin, Matin Amani, Terrence P O'Regan, A Glen Birdwell, and Madan Dubey		**5d. PROJECT NUMBER**
		5e. TASK NUMBER
		5f. WORK UNIT NUMBER
7. PERFORMING ORGANIZATION NAME(S) AND ADDRESS(ES) US Army Research Laboratory ATTN: RDRL-SER-L 2800 Powder Mill Road Adelphi, MD 20783-1138		**8. PERFORMING ORGANIZATION REPORT NUMBER** ARL-TR-7399
9. SPONSORING/MONITORING AGENCY NAME(S) AND ADDRESS(ES)		**10. SPONSOR/MONITOR'S ACRONYM(S)**
		11. SPONSOR/MONITOR'S REPORT NUMBER(S)

12. DISTRIBUTION/AVAILABILITY STATEMENT

Approved for public release; distribution unlimited.

13. SUPPLEMENTARY NOTES

14. ABSTRACT

The effect of titanium oxide (TiO_2) thickness on hysteresis behavior in non-volatile, metal-insulator-metal resistive random access memory (RRAM) was investigated using a $Zr_{40}Cu_{35}Al_{15}Ni_{10}$ (ZCAN) amorphous metal bottom electrode and an indium (In) top electrode. Due to the atomically flat nature of the amorphous ZCAN contact, the switching behavior of very thin metal oxides can be more accurately measured, unlike in aluminum (Al) or titanium (Ti) films, which typically have a surface roughness that is on the same order of magnitude as the dielectric thickness. TiO_2 grown by atomic layer depositions (ALD) was used as the dielectric layer and has previously been used with platinum (Pt) electrodes to demonstrate RRAM devices with high on/off ratios. We found that at higher thickness, the ALD TiO_2 transforms from an amorphous film to an anatase film, which plays a critical role for the hysteresis and switching characteristics in these devices.

15. SUBJECT TERMS

Metal-insulator-metal structures, memristors, resistive random access memory, RRAM, titanium dioxide, $Zr_{40}Cu_{35}Al_{15}Ni_{10}$, ZCAN, resistive memory, tunnel junction

16. SECURITY CLASSIFICATION OF:			**17. LIMITATION OF ABSTRACT**	**18. NUMBER OF PAGES**	**19a. NAME OF RESPONSIBLE PERSON** Matthew L Chin
a. REPORT Unclassified	**b. ABSTRACT** Unclassified	**c. THIS PAGE** Unclassified	UU	18	**19b. TELEPHONE NUMBER (Include area code)** (301) 394-2830

Standard Form 298 (Rev. 8/98)
Prescribed by ANSI Std. Z39.18

Contents

List of Figures

List of Tables

1. Introduction

Resistive-switching memory elements based on metal-insulator-metal (MIM) diodes have attracted great interest due to their potential as components for simple, inexpensive, and high-density non-volatile storage devices. MIM diodes composed of a thin metal oxide layer sandwiched between 2 metal layers are ideal for cross-point memory arrays, which are typically composed of 1 MIM stack and 1 resistor per unit, and organized in word and bit-lines. This design allows for the smallest memory cell size of $4F^2$, where F is the minimum feature size. Such resistive-switching memory elements, also popularly referred to as resistive random access memory (RRAM), were previously fabricated using various transition metal oxides as the insulator layer, including titanium oxide (TiO_2), niobium pentoxide (Nb_2O_5), nickel(II) oxide (NiO), strontium titanate ($SrTiO_3$), strontium zirconate ($SrZrO_3$), barium titanate ($BaTiO_3$), lead titanate ($PbTiO_3$), and aluminum oxide (Al_2O_3).[1–13]

Much of the previously published works on TiO_2-based resistive-switching devices speculate that the resistive switching is due to 1 of 2 possible mechanisms. A number of groups postulate that the formation of conducting filaments rich with oxygen vacancies form through electromigration when a large potential is applied across the film. This purportedly causes a significant drop in the 2-terminal resistance.[4–7,9] With an exponential increase in current density due to these conductive filaments, localized heating within the filaments causes thermal rupturing, which then leads to their destruction, and thus brings the 2-terminal resistance back to a higher state. In the second suggested mechanism, the applied bias to the RRAM structure leads to an increase or decrease of defects at the TiO_2/metal interface (possibly from oxygen ion migration), which changes the Schottky barrier height.[1,2]

Earlier work focused on fabricating TiO_2 RRAM structures using oxide films grown or deposited either by thermal or plasma oxidation of a Ti metal film or e-beam deposition of TiO_2 granules, or through radio frequency (RF) reactive sputtering.[1–3,11] These methods typically result in material with very poor thickness control, low uniformity, significant porosity, and high defect densities. On the other hand, atomic layer deposition (ALD) allows for precise control of the layer thickness and can produce higher quality films with very uniform coverage.[5–7,9]

To support the study of thin TiO_2 films, a $Zr_{40}Cu_{35}Al_{15}Ni_{10}$ (ZCAN) amorphous metal was used as the bottom anode electrode due to its relatively low surface roughness (typically ranging from 0.2 to 0.5 nm root mean square [RMS] as measured by atomic force microscopy).[14] The low surface roughness allows for thinner insulator layers, on the order of 1 to 10 nm, to be deposited on top of the bottom electrode with minimal risk of pinholing due to the roughness of the metal film, which in some cases can be on the same order of magnitude as the dielectric thickness. Al films, for example, can have a roughness of over 40 nm RMS.[14] Due to the atomically flat nature of ZCAN, significant improvements in device reproducibility can be realized compared to most crystalline metals. Various metals were reviewed for the top cathode metal, and all were selected to have a lower work function compared to ZCAN, which has a metal work function of ~4.8 eV.[14] This asymmetry in the electrodes has been found to promote Fowler-Nordheim tunneling, which assists with providing desirable current asymmetry in the current-voltage (I-V) characteristics of the MIM diode.

In this report, we explore how the thickness of an ALD-deposited TiO_2 dielectric layer affects the RRAM electrical properties, which could help uncover the switching mechanism and lead to lower variability in massive RRAM arrays. Thicknesses of 5, 10, and 20 nm were reviewed, using a ZCAN bottom anode and an indium (In) top cathode. In was used as the cathode electrode due to its relatively high on/off ratios as determined by experimentation with different cathode metals. In metal has a reported work function of ~4.1 eV.[15]

2. Experimental Procedure

All devices used in this study were fabricated on silicon (Si) substrates with a 300-nm layer of thermally grown silicon dioxide (SiO_2). ZCAN films were then deposited to a thickness of 250 to 350 nm using a DC sputtering process with a chamber argon (Ar) pressure of 5 mTorr at 60 W. The TiO_2 was grown using a thermal ALD process operating at 200 °C for thicknesses of 5, 10, and 20 nm using de-ionized water (H_2O) and tetrakis(dimethylamido)titanium (TDMAT) heated to 95 °C as the precursors. The thickness was confirmed using ellipsometry of equivalent films grown on Si substrates. The In top electrode was deposited using thermal evaporation, on samples patterned using contact photolithography based on the AZ 5214E reverse-image photoresist. X-ray photoelectron spectroscopy (XPS) was performed to confirm the composition of the TiO_2 films. Confocal Raman spectroscopy was used to determine the morphology and uniformity of the TiO_2 films, and was measured using the 532-nm line of a frequency-doubled neodymium (Nd): yttrium aluminum garnet (YAG) laser as the excitation source at a power density of 11 mW/μm^2 (Fig. 1).[17]

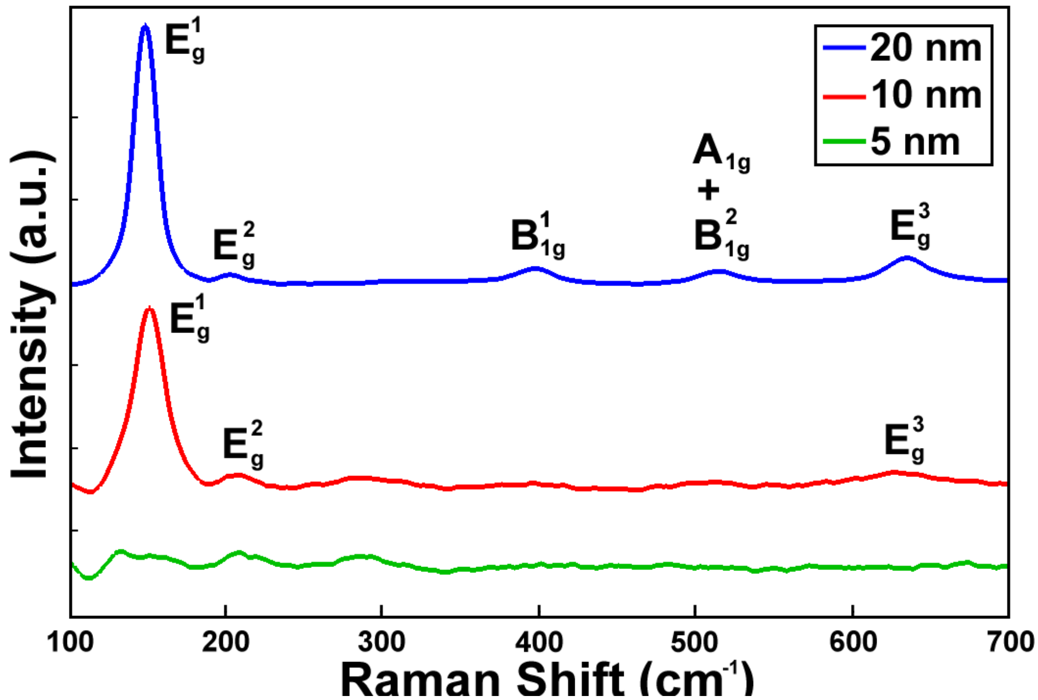

Fig. 1 Background-subtracted Raman spectra of 5-, 10-, and 20-nm-thick TiO_2 films grown on a ZCAN bottom electrode are shown with the intensity showing a correlation with oxide thickness

The devices were measured in a cryogenic probe station in a pure nitrogen (N_2) atmosphere at 298 K. A Keithley 4200 semiconductor characterization system was used to extract the electrical properties via current density-voltage (J-V) sweeps, varying the voltage and measuring current over several preset ranges including ±1, ±2, and ±2.5 V. The ratio of the resistance in the high resistance state (HRS) over the low resistance state (LRS) was derived from the J-V curves. Additionally, we performed an electro-forming step on all devices, which was carried out as a voltage sweep with a compliance current of 1 A/cm^2. Several devices were measured for each device set and each device was manually cycled over 25 times in order to obtain repeatable and consistent J-V characteristics for the batch. Bipolar resistive switching was observed in all measured devices, and a representative J-V curve including the individual sweeps is highlighted in Fig. 2.

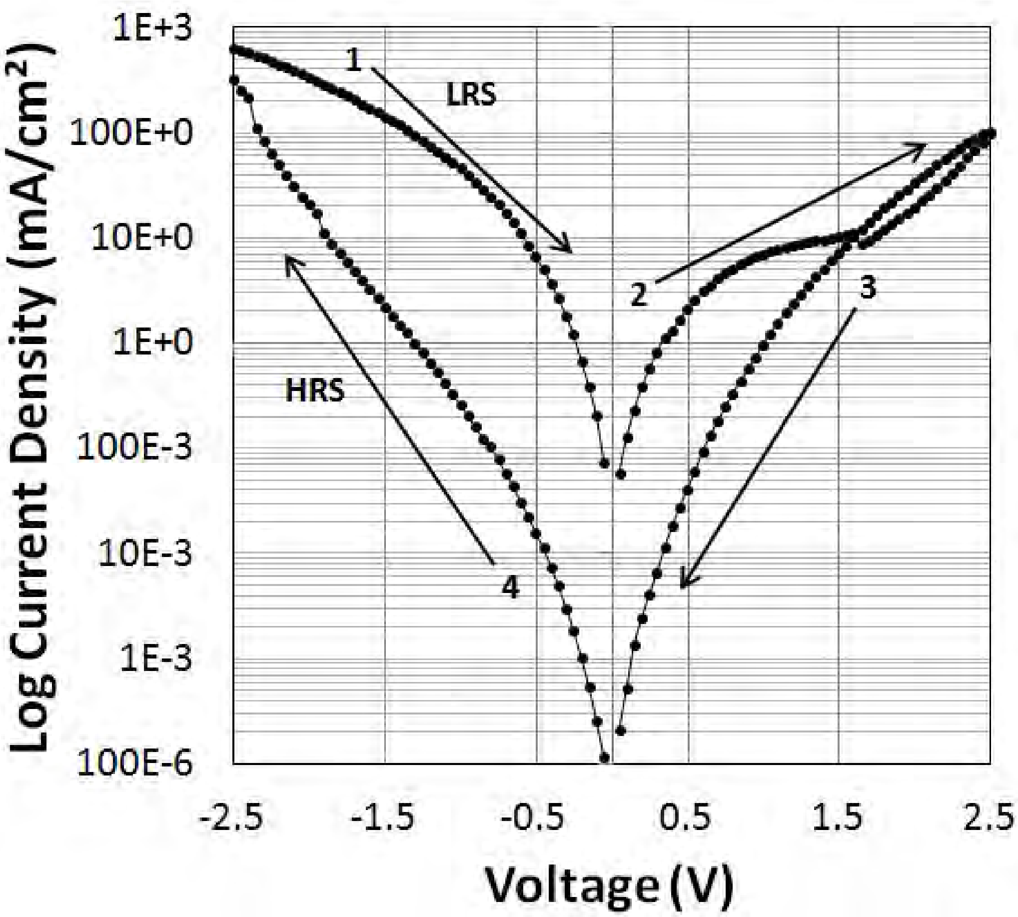

Fig. 2 **J-V curve with the hysteretic sweep order represented by arrows on the plot. The device shown here is 60 µm x 60 µm in area, with a 250-nm-thick layer of ZCAN as the anode, a 20-nm-thick layer of TiO_2, and a 300-nm-thick layer of In as the cathode.**

3. Results and Discussion

The devices in this study had relatively low breakdown voltages ranging from –2 to –3.5 V depending on the insulator thickness. This is likely due to the fact that these ALD-grown films were significantly thinner than their counterparts in the literature. Varying the oxide thickness of the MIM structures provided surprising results. Figure 3 provides a log plot comparing the J-V characteristics of ZCAN/TiO_2/In diodes with different insulator thicknesses. Current density increases as the TiO_2 thickness increases. This appears counterintuitive, as an increase in oxide thickness would exponentially reduce tunneling current.

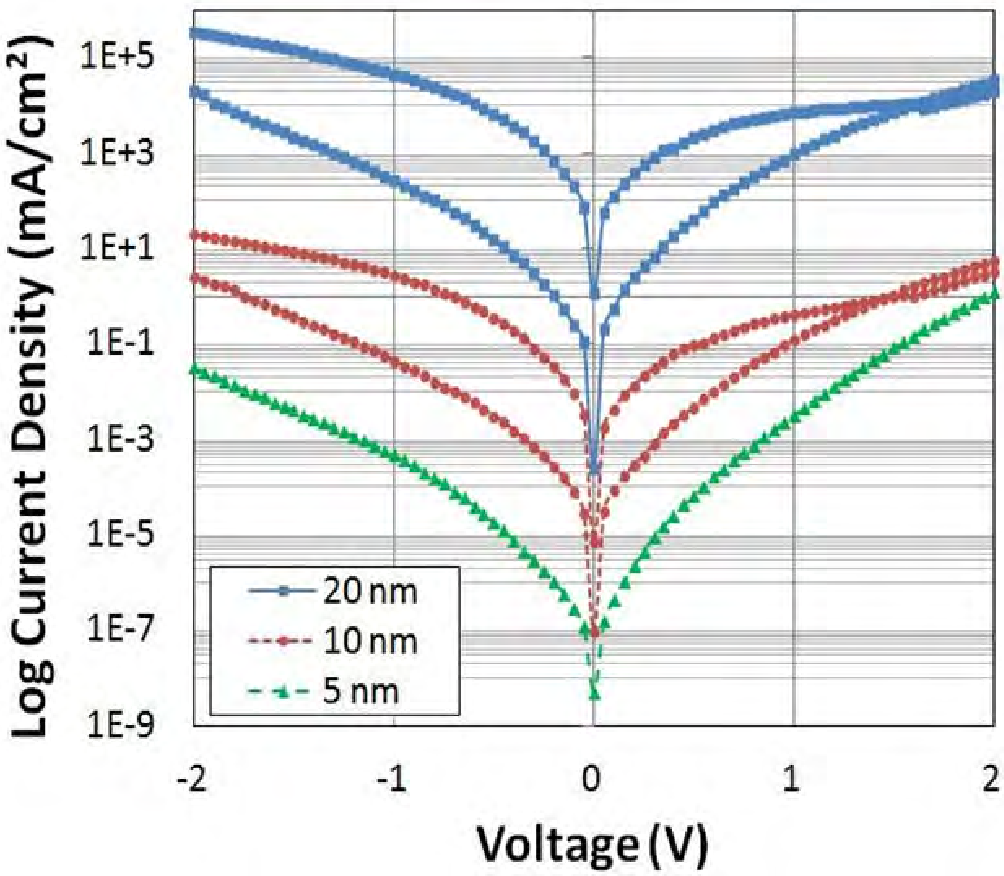

Fig. 3 Hysteretic J-V curves for 3 devices for TiO_2 insulator thicknesses of 5, 10, and 20 nm

Raman spectroscopy was used to determine the morphology of the 5-, 10-, and 20-nm TiO_2 films. The 10- and 20-nm films exhibited Raman spectra typical of an anatase phase. Using the frequency from the Raman measurement, full-width half-maximum (FWHM) of the E^1_g mode from the Raman analysis, correlated Raman, and XRD results by Zhang et al., we calculated the grain size to be 4.7±0.5 and 8.1±0.5 nm for the 10- and 20-nm films, respectively.[16,17] On the other hand, the 5-nm-thick films were found to be amorphous. We note that the blueshift and broadening of the FWHM of the E^1_g mode may also be attributed to a combined mechanism involving both phonon confinement and non-stoichiometry effects.[16]

We observe a hysteresis increase with increased oxide thickness as shown in Table 1. In the MIM structure with a 5-nm-thick TiO_2 layer, there is little hysteresis present, but in the 10- and 20-nm MIM structures, a significant R_{on}/R_{off} ratio was produced. The R_{on}/R_{off} ratio as a function of applied voltage is shown in Fig. 4. We believe that the absence of an apparent hysteresis at the lower dielectric thicknesses is related amorphous structure of our 5-nm ALD films and the lower throughput current. For thicker films, we propose that the anatase phase of TiO_2 promotes the formation of conductive filaments, allowing the film to enter a lower resistance state.

Table 1 Hysteresis, asymmetry, and current density for MIM structures based on a ZCAN/TiO_2/In stack with varying TiO_2 thickness

Oxide Thickness	5 nm	10 nm	20 nm
Maximum hysteresis	1.1 at –1.35 V	129 at –350 mV	786 at –100 mV
Asymmetry (off state) at 1 V	6.9	6.8	6.5
Asymmetry (on state) at 1 V	N/A	2.7	3.8
Current density (mA/cm^2) at 1 V (off state)	316	403	692

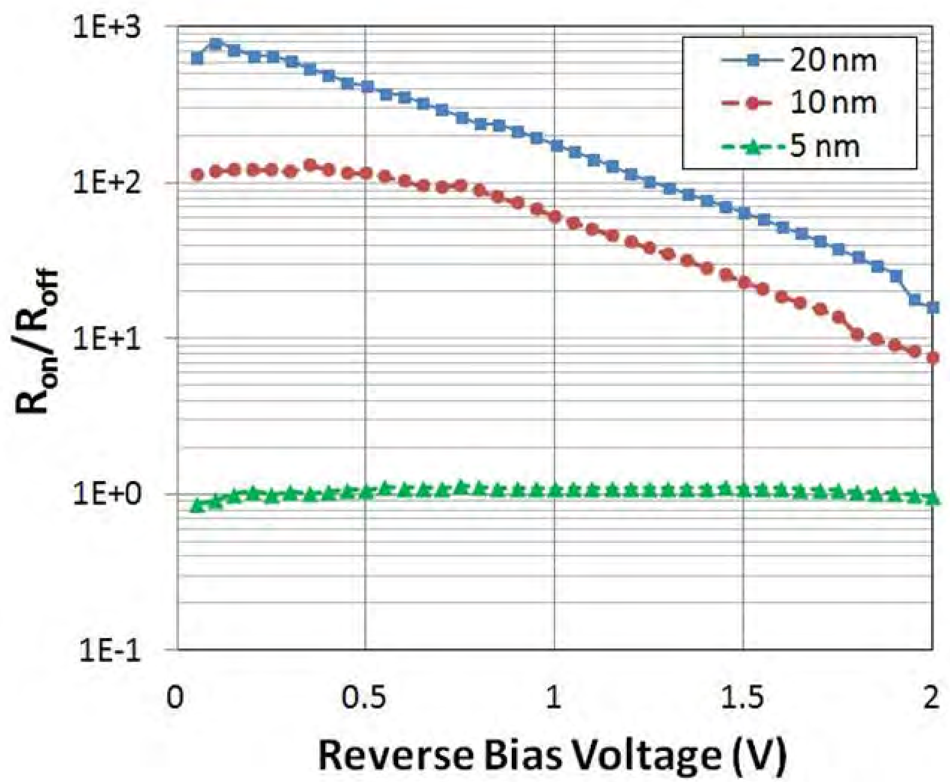

Fig. 4 The R_{on}/R_{off} ratios as a function of reverse bias voltage for TiO_2 insulator thicknesses of 5, 10, and 20 nm

4. Conclusion

In this study, we fabricated and characterized several ZCAN/TiO_2/In MIM resistive memory cells with varying oxide thickness. Since our films were fabricated using an ALD process in conjunction with an atomically smooth bottom electrode, we were able to track the effects of thickness on the current density in these devices, which has not been previously reported on. We were able to show that increasing the TiO_2 thickness results in an increase in the current density for the devices, which we correlated to the increased ratio of anatase-to-amorphous TiO_2 as well as increasing crystal size, which contributes to conduction through the bulk film, reducing the impact of filament formation.

5. References

1. Huang J-J, Kuo C-W, Chang W-C, Hou T-H. Transition of stable rectification to resistive switching in Ti/TiO2/Pt/Oxide. Appl. Phys. Lett. Jun 2010.2;96(26):262901 (1–3).

2. Yarmarkin VK, Shul'man SG, Lemanov VV. Resistive switching in Au/TiO2/Pt thin film structures on silicon. Phys. Solid State. Feb 2008;50(10):1841–1847.

3. Villafuerte M, Juarez G, Heluani SP, Comedi D. Hysteretic current–voltage characteristics in RF-sputtered nanocrystalline TiO2 thin films. Phys. B Condens. Matter. Sep 2007;398(2):321–324.

4. Rohde C, Choi BJ, Jeong DS, Choi S, Zhao J-S, Hwang CS. Identification of a determining parameter for resistive switching of TiO2 thin films. Appl. Phys. Lett. Jun 2005;86(26):262907 (1–3).

5. Kim KM, Choi BJ, Jeong DS, Hwang CS, Han S. Influence of carrier injection on resistive switching of TiO2 thin films with Pt electrodes. Appl. Phys. Lett. Oct 2006;89(16):162912 (1–3).

6. Choi BJ, Jeong DS, Kim SK, Rhode C, Choi S, Oh JH, Kim HJ, Hwang CS, Szot K, Waser R, Reichenberg B, Tiedke S. Resistive switching mechanism of TiO2 thin films grown by atomic-layer deposition. J. Appl. Phys. Aug 2005;98(3):033715 (1–10).

7. Kim KM, Kim GH, Song SJ, Seok JY, Lee MH, Yoon JH, Hwang CS. Electrically configurable electroforming and bipolar resistive switching in Pt/TiO2/Pt structures. Nanotechnology. Jul 2010;21(30):305203 (1–7).

8. Jeong DS, Schroeder H, Waser R. Mechanism for bipolar switching in a Pt/TiO_{2}/Pt resistive switching cell. Phys. Rev. B. May 2009;79(19):195317.

9. Kim GH, Lee JH, Seok JY, Song SJ, Yoon JH, Yoon KJ, Lee MH, Kim KM, Lee HD, Ryu SW, Park TJ, Hwang CS. Improved endurance of resistive switching TiO2 thin film by hourglass shaped Magn[e-acute]li filaments. Appl. Phys. Lett. Jun 2011;98(26):262901–3.

10. Shin J, Kim I, Biju KP, Jo M, Park J, Lee J, Jung S, Lee W, Kim S, Park S, Hwang H. TiO2-based metal-insulator-metal selection device for bipolar resistive random access memory cross-point application. J. Appl. Phys.Feb 2011;109(3):033712–4.

11. Joeng DS, Schroeder H, Breuer U, Waser R. Characteristic electroforming behavior in Pt/TiO2/Pt resistive switching cells depending on atmosphere. J. Appl. Phys. Dec 2008;104(12):123716–8.

12. Yanagida T, Nagashima K, Oka K, Kanai M, Klamchuen A, Park BH, Kawai T. Scaling effect on unipolar and bipolar resistive switching of metal oxides, Sci. Reports. Apr 2013;3.

13. Sawa A. Resistive switching in transition metal oxides. Mater. Today. Jun 2008;11(6)28–36.

14. Cowell III EW, Alimardani N, Knutson CC, Conley Jr JF, Keszler DA, Gibbons BJ, Wager JF. Advancing MIM electronics: Amorphous metal electrodes. Adv. Mater. Jan 2011;23(1)74–78.

15. Michaelson HB. The work function of the elements and its periodicity. J. Appl. Phys. Nov 1977;48(11)4729–4733.

16. Zhang WF, He YL, Zhang MS, Yin Z, Chen Q. Raman scattering study on anatase TiO2 nanocrystals. J. Phys. D: Appl. Phys. Apr 2000;33:912–916.

17. Frank O, Zukalova M, Laskova B, *et al*. Raman spectra of titanium dioxide (anatase, rutile) with identified oxygen isotopes (16, 17, 18). Phys. Chem. Chem. Phys. Sep 2012;4:14567–14572.

List of Symbols, Abbreviations, and Acronyms

Al	aluminum
Al_2O_3	aluminum oxide
ALD	atomic layer deposition
Ar	argon
$BaTiO_3$	barium titanate
FWHM	full-width half-maximum
H_2O	water
HRS	high resistance state
In	indium
I-V	current-voltage
J-V	current density-voltage
LRS	low resistance state
MIM	metal-insulator-metal
N_2	nitrogen
Nb_2O_5	niobium pentoxide
Nd	neodymium
NiO	nickel(II) oxide
$PbTiO_3$	lead titanate
Pt	platinum
RF	radio frequency
RMS	root mean square
RRAM	resistive random access memory
Si	silicon
SiO_2	silicon dioxide
$SrTiO_3$	strontium titanate
$SrZrO_3$	strontium zirconate

TDMAT	tetrakis(dimethylamido)titanium
Ti	titanium
TiO_2	titanium oxide
XPS	x-ray photoelectron spectroscopy
YAG	yttrium aluminum garnet
ZCAN	$Zr_{40}Cu_{35}Al_{15}Ni_{10}$

1 DEFENSE TECH INFO CTR
(PDF) ATTN DTIC OCA

2 US ARMY RSRCH LAB
(PDF) ATTN IMAL HRA MAIL & RECORDS MGMT
ATTN RDRL CIO LL TECHL LIB

1 GOVT PRNTG OFC
(PDF) ATTN A MALHOTRA

1 US ARMY NATICK SOLDIER RESEARCH DEVELOPMENT
(PDF) AND ENGINEERING CENTER
NANOMATERIALS SCIENCE TEAM
ATTN AMSRD NSR WS B NS R OSGOOD

4 US ARMY RSRCH LAB
(PDF) ATTN RDRL SER E
G BIRDWELL
T O'REGAN
ATTN RDRL SER L
M CHIN
M DUBEY